Energy 244 (2022) 122623

Contents lists available at ScienceDirect

Energy

journal homepage: www.elsevier.com/locate/energy

An interval quantification-based optimization approach for wind turbine airfoil under uncertainties

Xinzi Tang [a, *], Keren Yuan [a], Nengwei Gu [a], Pengcheng Li [b], Ruitao Peng [a]

[a] Research Center of Wind Turbine Technology & Equipment, School of Mechanical Engineering, Xiangtan University, Xiangtan 411105, China
[b] Ming Yang Smart Energy Group Limited, Zhongshan 528437, China

ARTICLE INFO

Article history:
Received 7 April 2021
Received in revised form
7 November 2021
Accepted 12 November 2021
Available online 15 November 2021

Keywords:
Wind turbine
Optimization
Turbulence intensity
Geometric error
Interval
Surrogate model

ABSTRACT

Wind turbine airfoil operates in the atmosphere with uncertain turbulence and relatively low Reynolds number all year round. Meanwhile, due to the complexity of blade airfoil fabrication, there are inevitable geometric deviations to the theoretical airfoil shape. These uncertainties from manufacturing and operating environment couple together and lead to performance degradation. In the traditional wind turbine airfoil design process, the uncertainties are not the design variables, objectives, and constraints are deterministic. This paper presents a novel approach for uncertain analysis and aerodynamic robustness optimization of wind turbine airfoil considering turbulence and geometric error uncertainties. An interval method coupled with the Kriging model is applied to quantify the uncertain influence, and is integrated in the optimization. The target of optimization is to find an optimal airfoil with low sensitivity to uncertainties, as well as maintaining lift to drag ratio. After optimization the min std best airfoil shows 17.96% reduction of fluctuation range and no decreased average of lift to drag ratio compared to the baseline airfoil. The optimization was validated through flow field analysis by non-deterministic CFD approach. The proposed methodology can be further applied to other engineering designs making product less sensitivity to uncertainties thus more reliable.

1. Introduction

Wind energy as one of the most promising renewable energy has attracted great attention and wind power technology has developed rapidly all over the world. Wind turbine design has been in pursuit of more efficient, stable, and reliable. Wind turbines often operate in the atmosphere with high turbulence intensity and uncertainty all year round [1]. The uncertain characteristics of the operating environments and wind turbine blade airfoil have a significant impact on the stability and reliability of wind power [2]. Small change and disturbance in airfoil aerodynamics leads to large performance deviation of wind turbine. In practice, manufacturers try to mitigate aerodynamic uncertainties by ensuring tight controls on the tolerances of blade geometry during manufacturing and handling [3]. However, this approach not only increases the cost of wind power but also makes it difficult to achieve due to the complexity and dispersion of the manufacturing and handling process. A well-designed airfoil generates high lift low drag as well as less sensitivity to stochastic disturbance is critical to wind turbine design.

Several researches have been focused on the robustness design of rotorcraft and helicopter airfoils. The problem of robustness has been addressed and discussed from the point of view of the flow solver, the mesh deformation, and the design variable parametrization [4]. The objective of robust optimization is to design an airfoil that is minimally sensitive to the variation of the operating conditions such as Mach number and angle of attack [5]. As for wind turbine airfoil, two main kinds of uncertainties can be concluded as stochastic turbulent operating conditions at low Reynolds number and geometric errors. The operational condition uncertainty relates to the incoming inflow which is nature, random and uncontrollable such as turbulence intensity. The atmospheric instability increases the fluctuation of annual energy production and aggravates the fatigue failure of wind turbine [6]. The geometric error occurs due to icing, dust, or manufacturing factors, such as the inevitable uncertainty from process method, material, and equipment in the production process of wind turbine blade, including the fibre-laying, resin curing, adhesive bonding, and surface coating processes. The slight change in the airfoil geometry

* Corresponding author.
E-mail address: tangxinzi@xtu.edu.cn (X. Tang).

https://doi.org/10.1016/j.energy.2021.122623
0360-5442/

causes apparent airflow disturbance, which leads to rapid deterioration of aerodynamic performance [7]. These uncertainties do not exist alone but often couple together. The coupling effects of multiple uncertainties during operation may lead to severe performance discrepancy, which cannot be ignored.

In the traditional wind turbine airfoil design optimization process, the design variables, objectives, and constraints are deterministic. The influence of uncertain factors cannot directly be included or the design is simplified as multi point design. The optimal solution of deterministic optimization design tends to be very sensitive to the uncertainties occurred in operation.

Robust design methodology has been developed to minimize the sensitivity to uncertainties in product and system process design. Aerodynamic robustness optimization (ARO) is a relative new subject in wind turbine technology. The basic idea of ARO is to minimize the impact of uncertain factors on aerodynamic performance through design optimization. In the ARO process, there are two difficulties embedded: one is how to define the multiple uncertainties, i.e., to identify the types of uncertainties and establish the joint density distributions, and the other is how to couple the massive uncertain analysis in the optimization effectively. Considering uncertainties of nature flow turbulence and geometric errors, different types of uncertainties can be defined according the internal attributions of variables. As in Ref. [8], the turbulence intensity was described as a random variable using a normal distribution. As for wind turbine airfoil, a variety of parameterization methods have been used in geometry definition, such as class-shape function transformation (CST) method [9], free-form deformation (FFD) method [10], Hicks-Henne functions (H−H) [11], and PARSEC [12], etc. Considering geometric error, for precise description of the airfoil shape complexity and sensitivity to disturbance, many variables are often included in parameterization to avoid losing key geometric information [13]. Researchers also used Gaussian distribution to define the geometric error [14]. From above, wind turbine airfoil related uncertainty analysis becomes a stumbling block in ARO, due to multiple types of uncertainties and high dimension of uncertain input parameters.

To overcome the obstacle of definition of multiple uncertainties, a novel interval method is proposed in this paper. The interval method describes the uncertainty as an upper and lower limit, avoiding density distribution modelling when only the limit values are focused, thus makes the uncertainty quantification efficient. This method origins from structure reliability analysis [15–17], there is however rare application in airfoil optimization robust design.

The ARO is a multi-layer optimization process. The inner layer is the evaluation of objective function and limit function of the extreme cases, the middle layer is the uncertainty analysis of objective function and limit function of the extreme cases, and the outer layer is the optimization process of the optimization target. Because of the execution of the inner and middle layers, a considerable computational burden is increased. Especially for low Reynolds wind turbine airfoil robustness optimization where boundary layer and transition flows are considered, the Reynolds Averaged Navier-Stokes (RANS) based computational fluid dynamics (CFD) simulation with refined surface mesh is inevitable, which needs computing resource and is time-consuming.

To couple the massive uncertain analysis in optimization and improve calculation efficiency, a Kriging surrogate model is established and integrated in ARO in this paper. Combined with Latin Hypercube Sampling (LHS), the Kriging model is capable to achieve an efficient and accurate fitting with less dependency on sample scale comparing to other models [18], such as polynomial chaos expansion (PCE) [19] and Conditional Generative Adversarial Neural Network [20] etc. The Kriging model combined with the interval method is then integrated in ARO optimization process. The methodology is validated by Monte Carlo method [21].

The main ideas of this paper are: The uncertain turbulence at low Reynolds number and the uncertain geometric error are generally not taken into account in the traditional airfoil design process, which leads to the deviation of actual performance. To the author's knowledge, there is lack of research for airfoil design with consideration of uncertain turbulence and geometric errors at low Reynolds number. This paper aims to present a non-deterministic design optimization (called ARO) approach of airfoil, and the target of the optimization is to find an optimal airfoil with low sensitivity to uncertainties, as well as maintaining lift to drag ratio under uncertain turbulence at low Reynolds number. In this paper, the performance uncertainty quantification of airfoil is conducted under uncertain turbulence at relatively low Reynolds number, and uncertain geometric error. To avoid probabilistic modelling of uncertain variables, the uncertainties are characterized by a novel interval method. For reducing the massive work of uncertainty quantification, which involves boundary transitional flow simulation at low Reynolds for the large-scale samples, the interval method and the Kriging model are integrated together. And then the massive uncertain quantification is rapidly conducted and thus efficiently integrated with the optimization considering both average performance and standard deviation of performance.

The purpose of this paper is to provide an effective approach for wind turbine airfoil robustness optimization considering the stochastic turbulent wind condition and geometric uncertainties. The main novelties of this paper are: (1) The uncertain turbulence and geometric errors are considered in the airfoil design at low Reynolds number. (2) The uncertainties are characterized by a novel interval method to avoid probabilistic modelling of uncertain variables. (3) Based on the interval method and the Kriging model, the massive uncertain quantification can be rapidly conducted and efficiently integrated with the optimization algorithm. The quantification of uncertain effects and optimization methodology can further assist in wind turbine design and reliability analysis. This method can also be applied to other engineering designs making product more less sensitivity to uncertainties, more reliable.

The proposed approach is demonstrated in this paper as follows: the methodology including the airfoil geometry parameterization, the numerical simulation, the interval analysis based on Kriging model, and verification, and the overall workflow of optimization procedure are presented in Section 2. The proposed approach is then implemented for a benchmarking of wind turbine airfoil S809. The uncertain influences on aerodynamic performance of airfoil S809 with different level of uncertainties and coupled effects are explored in Section 3. The aerodynamic robustness optimization process for airfoil S809 including the mathematical optimization model and solution are illustrated in Section 4. The multi-objective optimization is solved by the Non-dominated Sorting Genetic Algorithm (NSGA-II). The ARO results are compared with the deterministic optimization and validated by the Monte Carlo (MC) modelling. The optimization was validated through flow field analysis by non-deterministic CFD approach. The main conclusions are drawn in Section 5.

2. Methodology

2.1. Airfoil profile parameterization

The Hicks-Henne function [12] can obtain a smooth geometric shape and has the advantage of high accuracy and stability. It generates subtle perturbations based on the reference airfoil without nonphysical geometry, thus it is applicable and selected for airfoil profile parameterization in the manufacturing error

uncertainty analysis. The expressions of the Hicks-Henne function are described as follows:

$$y_{up}(x) = y_{0up}(x) + \sum_{k=1}^{k=n} c_k f_k(x) \tag{1}$$

$$y_{low}(x) = y_{0low}(x) + \sum_{k=1}^{k=n} c_{k+n} f_k(x) \tag{2}$$

$$f_k(x) = \begin{cases} x^{0.25}(1-x)e^{-20x}, (k=1) \\ \sin^3\left(\pi x^{e(k)}\right), (2 \le k \le n) \end{cases} \tag{3}$$

$$e(x) = \frac{\ln 0.5}{\ln x_k}, 0 \le x_k \le 1 \tag{4}$$

Where, the subscripts up and low represent the upper and lower airfoil respectively, 0 represents the reference airfoil, n represents the term number, c_k is the corresponding coefficient of each functional term.

Due to the geometric error near the leading edge has a more important influence on the airfoil [9], four parameters c_1, c_2, c_3, c_4 are selected as the uncertain variables. The airfoil non-dimensional chord length is set to 1, k is 2, x_2 is 0.05. According to the geometric profile accuracy standard GB/T25383-2010, the maximum tolerance of wind turbine blade airfoil profile is ± (0.002 × c) mm (c is chord length). The corresponding ranges of Hicks-Henne function coefficients c_1, c_2, c_3 and c_4 are [−0.008,0.008]. With such level of geometric uncertainty, the samples with leading edge uncertainties for airfoil S809 are shown in Fig. 1.

2.2. Numerical simulation and validation

The numerical simulation method based on the modified transition SST model was used to predict laminar flow separation for steady airfoil performance analysis. By improving the SST k-omega model, the modified intermittent factor of separation flow and the transport equation related to the turbulence transition criterion are added into the transition SST model, therefore the modified transition SST model has better applicability for flow separation prediction compared with the traditional S-A model, k-epsilon model, and k-omega model [22]. The Reynolds number is 3 × 10^5. The

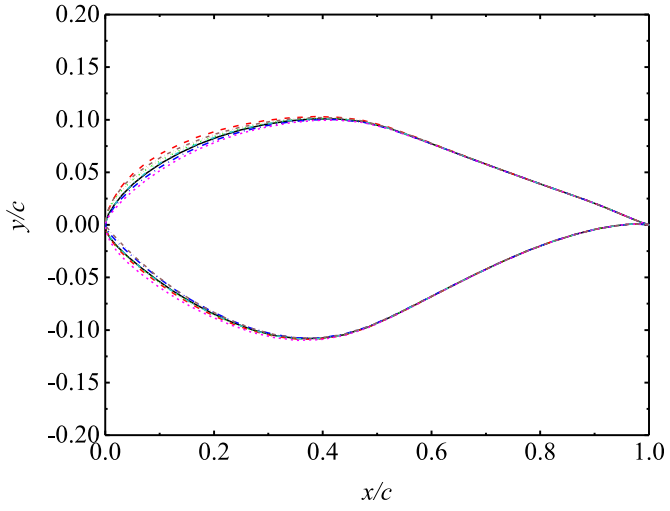

Fig. 1. Samples with leading edge uncertainties for airfoil S809.

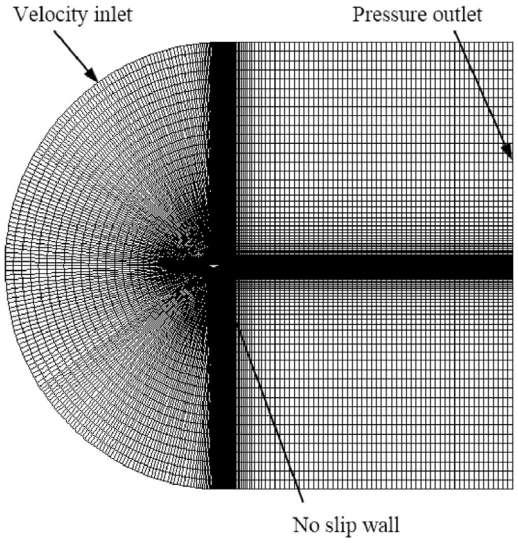

Fig. 2. Calculation domain and mesh of airfoil S809.

calculation domain for S809 is two-dimensional C type topology, as shown in Fig. 2. The length and width of which are 35 times chord length and 30 times chord length respectively. The rear length of the domain is 20 times chord length. The velocity inlet is defined for the inlet, where the incoming flow velocity and direction are given. The boundary condition of outlet is set as pressure outlet. The airfoil surface is regarded as no slip wall. The height of the first layer of grid near the wall is 10^{-5} times chord length, the normal growth rate is 1.1. The local fine mesh is carried out and y^+ is less than 1. Based on the grid independence study results shown in Table 1, a total number of 89700 grids is finally used. The pressure algorithm and the second-order upwind difference scheme are applied, and the convergence criterion of residual is less than 1 × 10^{-5}.

To validate the numerical simulation method, the calculated lift coefficients (C_l) and drag coefficients (C_d) based on the Transition SST model are compared with experimental results from CSU [23] and IET [24], as shown in Fig. 3. Good agreements between the CFD calculations and experimental results are obtained for the lift and drag coefficients. The numerical simulation method for lower angle of attack performance prediction is well validated. It is also noted that the discrepancy at high attack angle is mainly due to stall phenomenon which is not considered here.

2.3. Kriging model

A deterministic Kriging surrogate model is firstly established based on the numerical simulation which is validated with experimental results. Latin Hypercube Sampling (LHS) is used to generate samples within the design space. The LHS extracts sample points evenly and reduces the scale of the experiment, thus it obtains more comprehensive spatial information through fewer sample points compared to Monte Carlo (MC) sampling [25]. In the Kriging

Table 1
Grid independence study results.

	Grid number	Lift coefficient
Mesh1	67116	0.6691
Mesh2	89700	0.7706
Mesh3	104160	0.7781
Mesh4	120600	0.7755

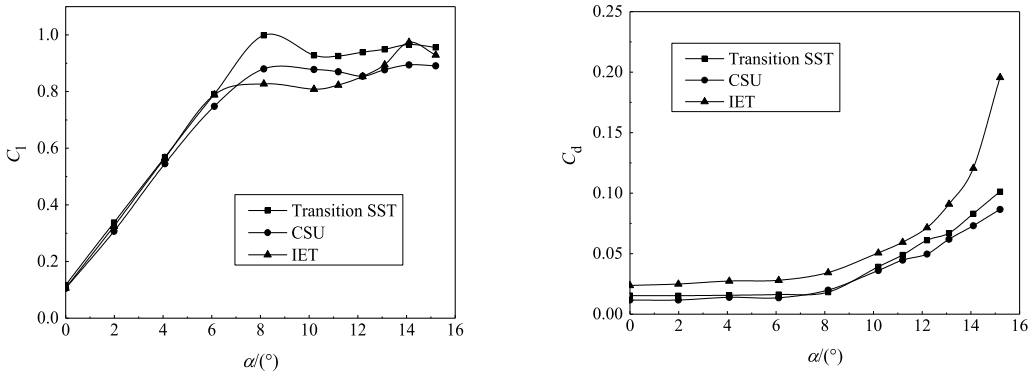

(a) Lift coefficient (b) Drag coefficient

Fig. 3. Validation of numerical simulation.

model, the relationship between the target system response value and independent variables can be predicted by making a sum of two components: one is the global approximation and the other is a variation component, which are expressed as follows [26,27]:

$$\begin{cases} y(x) = F(\beta, x) + z(x) \\ F(\beta, x) = f_1(x)\beta_1 + \cdots + f_p(x)\beta_p \end{cases} \tag{5}$$

Where, $y(x)$ is the target value, $F(\beta, x)$ is a regression model which forms the global design space fitting, usually using polynomial function, $z(x)$is the variation component usually known as correlation function, used to represent the local variation of the approximation in the design space,$\beta$is the corresponding regression coefficient, the covariance of which can be expressed as:

$$\mathrm{cov}\left[Z\left(x^i\right), Z\left(x^j\right)\right] = \sigma^2 R\left[R\left(x^i, x^j\right)\right] \tag{6}$$

Where$R$ is the correlation matrix and $R(x^i, x^j)$ represents the correlation function of any two sample points x^i andx^j. The Gaussian function is selected as the correlation function and its expression is:

$$R\left(x^i, x^j\right) = \exp\left[-\sum_{k=1}^{m} \theta_k \left|x^i{}_k - x^j{}_k\right|^2\right] \tag{7}$$

Where, m is the number of design variables and θ_k is the model parameter.

The determination coefficient R^2 measures the accuracy of the Kriging surrogate model, which can be expressed as:

$$R^2 = 1 - \frac{\sum_{i=1}^{n} (y_i - \widehat{y}_i)^2}{\sum_{i=1}^{n} (y_i - \overline{y})^2} \tag{8}$$

Where n is the number of test sample points, y_i is the experimental value, and$\widehat{y}_i$ is the estimated value of the surrogate model, $\overline{y}$is the mean of the experimental point set.

The Matrix of the Kriging model is shown in Table 2. Six parameters construct the variable vector, including the Hicks-Henne function coefficients, turbulence intensity and angle of attack, which is expressed as [c_1, c_2, c_3, c_4, TI, a]. The range of the Hicks-Henne function coefficients c_1, c_2, c_3 and c_4 is [−0.008,0.008]. The range of turbulence intensity TI and angle of attack α are [0.03,0.27] and [0°,10°], respectively. The response parameter is the lift to drag ratio, C_l/C_d. The total number of 80 samples were calculated by RANS CFD. The determination coefficient R^2 of the established Kriging model is 0.9710, which meets the accuracy requirement.

Table 2
Matrix of Kriging model.

Case No.	c_1	c_2	c_3	c_4	TI	α	C_l/C_d
1	0.0065	0.003	0.0075	0.0069	0.1415	1.9192	15.4
2	−0.0067	0.0053	−0.0035	−0.0038	0.0664	7.3737	34.6
3	−0.0028	0.008	0.0053	−8.08E-05	0.2676	10	24.7
4	−0.0064	0.0072	−0.0041	0.0075	0.0906	2.3232	20.4
5	−0.0059	0.004	0.0017	−0.008	0.2045	6.9697	26
…	…	…	…	…	…	…	…
80	−0.0015	−0.0062	−0.0046	−0.0078	0.1924	6.4646	23.8

2.4. Interval analysis method and validation

In order to obtain an efficient and reliable nonlinear multi-peak fitting for performance uncertainty quantitation under operational and geometric uncertainties, the interval analysis method combined with the Kriging surrogate model are employed.

The interval analysis method expresses the uncertainty quantification of each dimension as the interval form [28]:

$$A^I = \left[A^L, A^R\right] = \left\{x \middle| A^L \le x \le A^R, x \in R\right\} \tag{9}$$

Where, A^I, A^L, and A^R represent the interval, the lower bound of the interval, and the upper bound of the interval, respectively. The median value of the interval and the radius of the interval reflect the average size and stability of the variables respectively.

The median value of the interval A^C is defined as:

$$A^C = \frac{A^L + A^R}{2} \tag{10}$$

The radius of the interval A^W is defined as:

$$A^W = \frac{A^R - A^L}{2} \tag{11}$$

The median value and radius of the interval of the objective function are obtained by optimizing the maximized and minimized targets.

The quantitation process is mainly divided into three steps. Firstly, based on the airfoil profile parameterization, and the interval ranges of the Hicks-Henne function coefficients, the attack angle and the turbulence intensity are determined. Secondly, the deterministic Kriging model is established based on the LHS and

Table 3
Uncertainties comparison of lift to drag ratio of airfoil S809.

C_l/C_d	Upper limit	Lower limit	Median	Uncertainty range
Interval method	27.799	25.684	26.742	±1.057
Monte Carlo	27.627	25.514	26.571	±1.056
Discrepancy	0.62%	0.66%	0.064%	0.09%

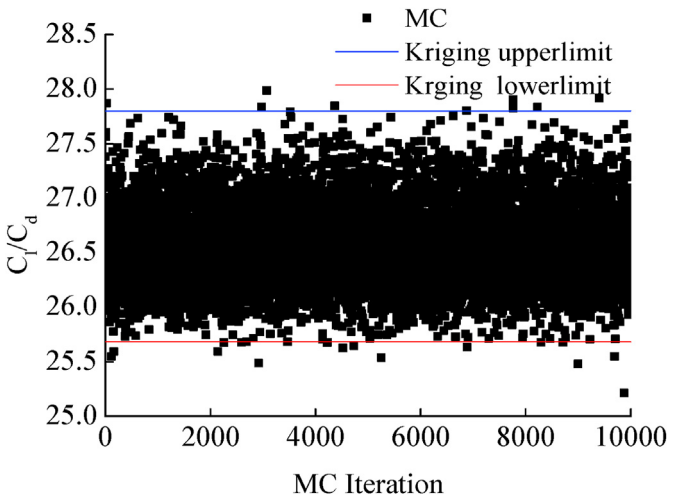

Fig. 4. Validation of interval analysis method.

RANS method. Thirdly, the upper limit and lower limit of the aerodynamic performance are searched based on the Kriging model and genetic algorithm, and the range and radius of the interval are obtained.

To further validate the uncertainty quantitation method, the interval analysis based on Kriging model with different sample scales were compared with Monte Carlo (MC) method with 10000 samples. An adequate sample scale is selected based on the sample size independence analysis. The airfoil is S809 and the Reynolds number is 3×10^5. The angle of attack is 6°. The uncertain parameter is *TI*. The variable range of median *TI* is [0.1725, 0.1275]. Table 3 and Fig. 4 compare the uncertain ranges of lift to drag ratio of airfoil S809 calculated by MC method and the interval analysis based on Kriging model with 80 samples. The uncertainty range of MC is defined as ±3σ. The uncertainty range of the interval and Kriging model is defined as ± interval radius. As shown in Fig. 4, the upper limit and lower limit of the interval analysis based on Kriging model exhibits good consistency to the results of MC method. The discrepancy of uncertainty range is 0.09% between the interval calculation and the MC results. It is therefore approved that the proposed interval analysis method has preferable accuracy.

2.5. Optimization design procedure

Based on the uncertainty quantitation, an ARO approach of wind turbine airfoil is put forward. Fig. 5 shows the overall workflow of the ARO procedure. The ARO is processed as three steps: Firstly, parameterize the airfoil geometry and determine input parameters and range, then establish the Kriging model based on LHS and low-Reynolds-number flow RANS CFD simulation. Secondly, search the upper limit and lower limit of the interval of the performance intervals based on generic algorithm and the Kriging model. Thirdly, establish the ARO optimization model and solve the multi-objective

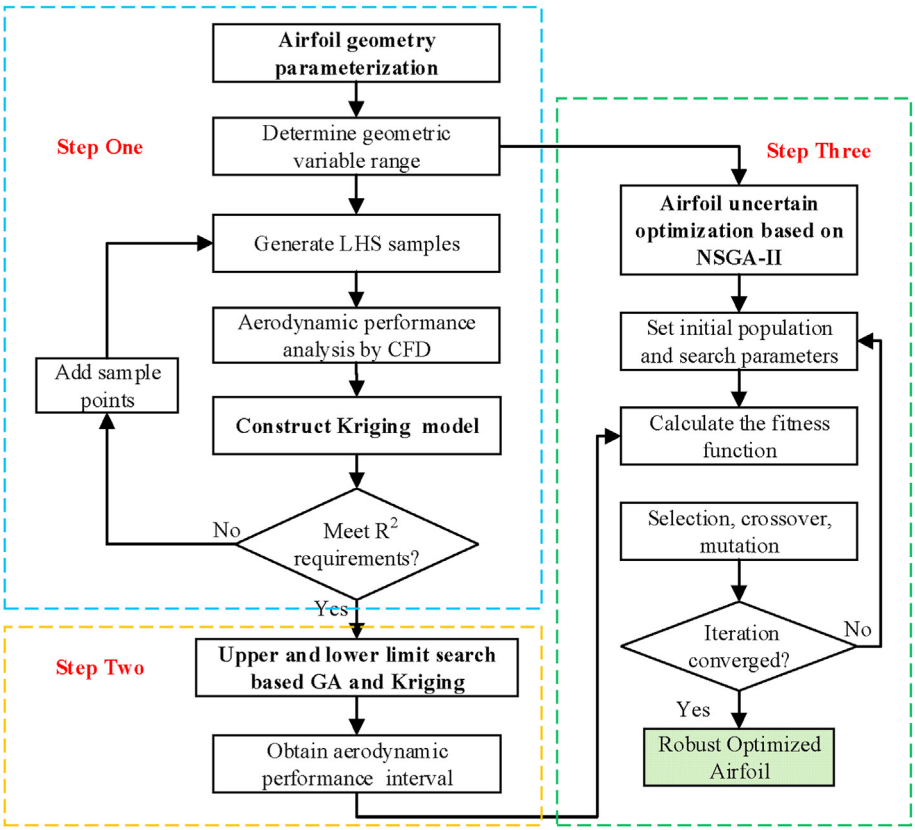

Fig. 5. Work flow of aerodynamic robustness optimization of airfoil.

optimization problem using non dominated sorting genetic algorithm NSGA-II.

3. Uncertain quantification of airfoil aerodynamic performance

3.1. Stochastic turbulence intensity

In the atmospheric boundary layer, the mean turbulence intensity (*TI*) is generally between 10% and 20%. With three median values and different uncertain levels of *TI*, the fluctuation ranges of lift to drag ratio of airfoil S809 were obtained by interval analysis method, as shown in Table 4 and Fig. 6. The angle of attack is 6° where the maximum lift to drag occurs. As shown in Fig. 6, for all cases, when the uncertainty represented by the interval radius of turbulence intensity increases, the fluctuation range of the lift to drag ratio of airfoil increases, which means that the aerodynamic stability of airfoil significantly decreases with the increase of the uncertainty of *TI*. It is also noted that the uncertainty effect is decreased with the increase of median TI. With a median *TI* of 0.1, when the interval radius of *TI* is from 0.0225 to 0.09, the interval median of lift to drag ratio increases from 29.73 to 31.34 increasing by 5.42%, and the interval radius of lift to drag ratio increases from 1.64 to 6.2. The maximum deviation occurs in the case of median *TI* of 0.1 and interval radius of 0.09. The corresponding deviation range (radius divided by median) reaches to ±19.78%.

3.2. Uncertain leading-edge error

Table 5 and Fig. 7 show the fluctuation range of lift to drag ratio of airfoil S809 under five different uncertain levels of geometric errors at angle of attack 6° with *TI* of 0.15. Three different interval medians and five different radii of the coefficients $c_1 \sim c_4$ were investigated, representing different levels of geometric errors within the maximum tolerance of wind turbine blade airfoil profile±(0.002c) mm (c is chord length). As shown in Fig. 7, for all cases, when the uncertainty represented by the interval radius of c_k increases, the fluctuation range of the lift to drag ratio of airfoil increases. With a median value of 0, when the interval radius of c_k increases from 0.0015 to 0.0075, the interval median value of lift to drag ratio decreases from 26.39 to 24.28, decreasing by 8%, and the interval radius of lift to drag ratio increases from 0.92 to 6.25. It is interesting to notice that the median of the lift to drag decreases with the increase of the interval radius of c_k. The uncertainty of lift to drag ratio is not obviously changed along with the median value of c_k.

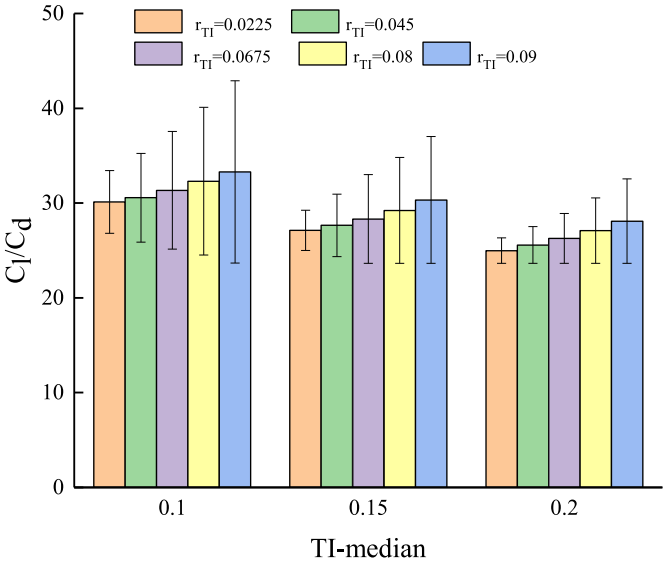

Fig. 6. Lift to drag ratios uncertainty of airfoil S809 under different *TI* uncertainties: r represents interval radius.

3.3. Coupling effect of uncertainties

Table 6 and Fig. 8 show lift to drag ratio of S809 airfoil at angle of attack of 0–10° under coupling effect of *ck* and *TI* uncertainties. The uncertain range of *ck* is [−0.0015, 0.0015] and the range of *TI* is [0.0375, 0.2625]. The Reynolds number is 3×10^5. With the increase of angle of attack, the median lift to drag ratio of airfoil increases gradually, while the uncertainty of lift to drag ratio increases first and then decreases slightly. The maximum uncertainty range of lift to drag ratio of airfoil occurs at the angle of attack of 4° while the maximum median exists at 7°. Results indicate that the airfoil is very sensitive to the coupled uncertainties at low angles of attack.

4. Aerodynamic robustness optimization and validation

4.1. Optimization mathematical model and solution parameter setting

The purpose of the ARO is to obtain an optimal airfoil with low sensitivity to geometric error and turbulence uncertainties, as well as maintaining lift to drag ratio at low Reynolds number. It is a multi-objective optimization problem, and there may be a

Table 4
Lift to drag ratio of airfoil S809 under different levels of turbulent intensity uncertainties.

TI				Lift to drag ratio			
Median	Uncertainties	Upper Limit	Lower Limit	Upper Limit	Lower Limit	Median	Uncertainties
0.1	±0.0225	0.1225	0.0775	31.38	28.09	29.73	±1.64
	±0.045	0.145	0.055	33.44	26.8	30.12	±3.32
	±0.0675	0.1675	0.0325	35.25	25.86	30.56	±4.69
	±0.08	0.18	0.02	36.48	25.42	30.95	±5.53
	±0.09	0.19	0.01	37.54	25.14	31.34	±6.2
0.15	±0.0225	0.1725	0.1275	27.8	25.68	26.74	±1.06
	±0.045	0.195	0.105	29.23	25.01	27.12	±2.11
	±0.0675	0.2175	0.0825	30.95	24.35	27.65	±3.30
	±0.08	0.23	0.07	32.07	23.83	27.95	±4.12
	±0.09	0.24	0.06	33.01	23.63	28.32	±4.69
0.2	±0.0225	0.2225	0.1775	25.51	24.15	24.83	±0.68
	±0.045	0.245	0.155	26.32	23.63	24.98	±1.34
	±0.0675	0.2675	0.1325	27.51	23.63	25.57	±1.94
	±0.08	0.28	0.12	28.24	23.63	25.94	±2.3
	±0.09	0.29	0.11	28.88	23.63	26.26	±2.63

Table 5
Lift to drag ratio of airfoil S809 under different levels of geometric error uncertainties.

c_k				Lift to drag ratio			
Median	Uncertainties	Upper limit	Lower limit	Upper limit	Lower limit	Median	Uncertainties
−0.0005	±0.0015	+0.001	−0.002	27.3	25.34	26.32	±0.98
	±0.003	+0.0025	−0.0035	27.99	23.89	25.94	±2.05
	±0.0045	+0.004	−0.005	28.71	22.15	25.43	±3.28
	±0.006	+0.0055	−0.0065	29.6	20.08	24.84	±4.76
	±0.0075	+0.007	−0.008	30.63	17.69	24.16	±6.47
0	±0.0015	+0.0015	−0.0015	27.31	25.47	26.39	±0.92
	±0.003	+0.003	−0.003	28.2	23.44	25.82	±2.38
	±0.0045	+0.0045	−0.0045	28.8	22	25.4	±3.4
	±0.006	+0.006	−0.006	29.51	20.37	24.94	±4.57
	±0.0075	+0.0075	−0.0075	30.53	18.03	24.28	±6.25
0.0005	±0.0015	+0.002	−0.001	27.3	25.6	26.45	±0.85
	±0.003	+0.0035	−0.0025	27.89	24.27	26.08	±1.81
	±0.0045	+0.005	−0.004	28.59	22.61	25.6	±2.99
	±0.006	+0.0065	−0.0055	29.43	20.65	25.04	±4.39
	±0.0075	+0.008	−0.007	30.43	18.37	24.4	±6.03

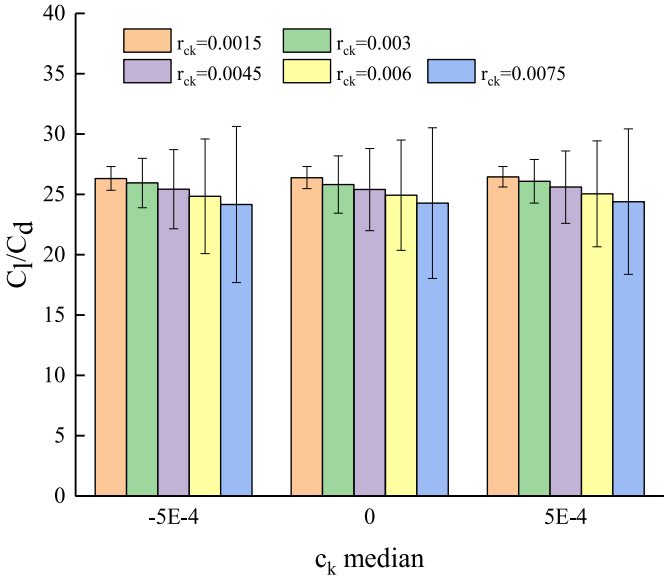

Fig. 7. Lift to drag ratio uncertainty of airfoil S809 with different c_k uncertainties: r represents interval radius.

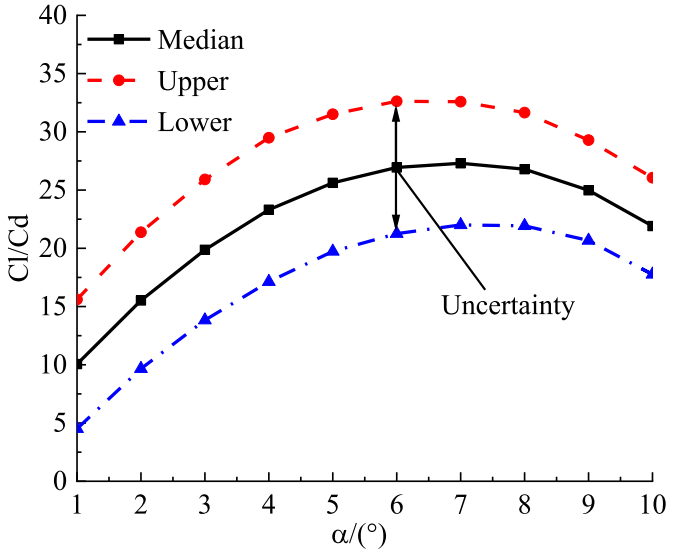

Fig. 8. Lift to drag ratio of airfoil S809 under uncertainties of turbulent intensity and geometric error.

compromise between maximizing the average of lift to drag ratio and minimizing the fluctuation range of lift to drag ratio. Thus the objectives of the ARO mathematical model are to maximize the average value of lift to drag ratio and to minimize the fluctuation range of lift to drag ratio, and the NSGA II is used to find the Pareto solutions. The baseline airfoil is S809 and the Reynolds number is 3×10^5. The angle of attack is 6°. The range of design variable c_k is [−0.006, 0.006]. The uncertain range of c_k is [−0.0015, 0.0015]. The variable range of median *TI* is [0.0375,0.2625]. A traditional deterministic optimization is also conducted for comparison purpose. The objective of deterministic optimization is set to maximize the lift to drag ratio.

The objectives and constraints of the ARO mathematical model are:

$$\begin{aligned} &Object: Maxmize\ m(C_l/C_d) \\ &\qquad\ Minmize\ r(C_l/C_d) \end{aligned} \tag{12}$$

$$s.t.: c_k \in [c_{k\min}, c_{k\max}] \tag{13}$$

Where m and r represent the median value and the interval radius of lift to drag ratio respectively, $C_{k\ min}$ and $C_{k\ max}$ are the upper and lower limits of C_k respectively. The initial population size is 200, the evolutionary algebra is 100, the crossover probability is 0.9, and the mutation probability is 0.01.

Table 6
Lift to drag ratio of airfoil S809 under turbulent intensity and geometric error uncertainties.

C_l/C_d	1°	2°	3°	4°	5°	6°	7°	8°	9°	10°
Upper limit	15.61	21.38	25.91	29.49	31.51	32.62	32.59	31.65	29.29	26.06
Lower limit	4.51	9.66	13.83	17.13	19.73	21.26	22.01	21.93	20.67	17.76
Median	10.06	15.52	19.87	23.31	25.62	26.94	27.3	26.79	24.98	21.91
Uncertainties	±5.55	±5.86	±6.04	±6.18	±5.89	±5.68	±5.29	±4.86	±4.31	±4.15

4.2. Optimal results and discussion

Fig. 9 plots the Pareto frontier of ARO. From the Pareto trend, it is obvious that there is a balance between to maximize the average of lift to drag ratio and to minimize the fluctuation range of lift to drag ratio. For further comparison purpose, three typical designs are selected, which are labelled as “Max aver Cl/Cd Best”, “Compromised Best” and “Min std Cl/Cd Best”. The “Max aver Cl/Cd Best” airfoil exhibits an maximized average of lift to drag ratio under turbulence, which is close to the deterministic optimization. The “Compromised Best” airfoil shows a compromised aerodynamic performance. The "Min std Cl/Cd Best" airfoil has a minimized lift to drag ratio fluctuations under turbulence with no decreased lift to drag ratio. The “compromised best airfoil” in Fig. 9 with both reduced interval radius and increased interval median is named as the ARO airfoil, and the deterministic optimal airfoil is named as the DO airfoil.

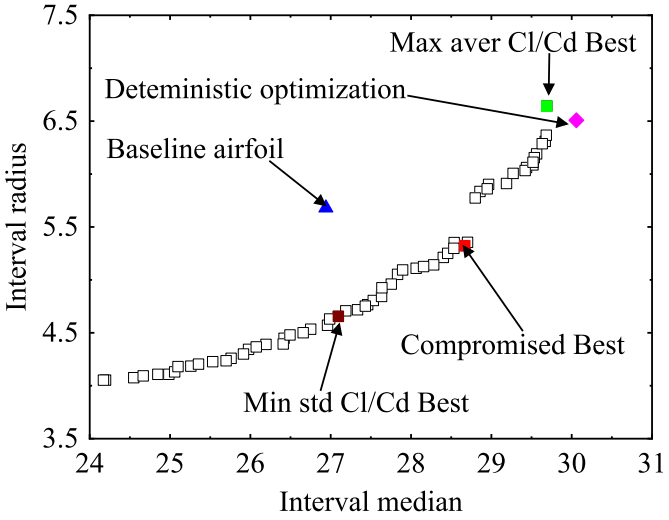

Fig. 9. Pareto frontier of ARO.

Table 7 presents the lift to drag ratio and uncertainty of lift to drag ratio of the baseline airfoil, the deterministic optimal airfoil (DO aifoil) and the selected designs under stochastic turbulence and geometric uncertainties. It can be seen from Table 7, for the “Max aver Cl/Cd Best” airfoil, the interval median of lift to drag ratio increases by 10.21% and the interval radius increases by 16.9% compared to the baseline airfoil. For the DO airfoil, the interval median of lift to drag ratio increases by 11.58% and the interval radius increases by 14.61%. For the “Min std Cl/Cd Best” airfoil, the interval radius decreases by 17.96%, with a slight increase of 0.56% for the interval median of lift to drag ratio, which indicates that the sensitivity to uncertainties is greatly reduced with no decreased lift to drag ratio after ARO optimization. While for the selected compromise design, the interval median of lift to drag ratio increases by 6.42% and the interval radius decreases by 6.34%.

Fig. 10 shows the geometric profile comparison between the compromised ARO airfoil (referred as ARO airfoil), the deterministic optimal airfoil and the baseline airfoil. It is exhibited in Fig. 9 that the profile at the leading edge of the compromised ARO airfoil is larger than the deterministic optimal airfoil and the baseline airfoil. The results indicate that a larger leading-edge profile tends to have a less sensitivity to uncertainties.

4.3. MC Validation for optimization

To further verify the optimization results, a Montel Carlo (MC) analysis with 10,000 samples was carried out for the above three airfoil profiles. Fig. 11 compares the calculated probability density distributions of lift to drag at angle of attack 6°. The uncertain range of c_k and TI are [−0.0015, 0.0015] and [0.0375,0.2625] respectively. The average lift to drag ratio of the ARO airfoil, the deterministic optimal airfoil and the baseline airfoil are 28.67, 30.06 and 26.94 respectively, while the standard deviations are 1.77, 2.17 and 1.89 respectively. It is evident that the ARO airfoil is less sensitive to the uncertain factors than the other two airfoil profiles. An optimized

Table 7
Comparison of lift to drag ratio and uncertainty under stochastic turbulence and geometric uncertainties.

Lift to drag ratio	Interval median	Uncertainty (Interval radius)	Increased rate of interval median	Increased rate of uncertainty
Baseline airfoil	26.94	5.68		
Max aver Cl/Cd Best airfoil	29.69	6.64	10.21%	16.9%
Min std Cl/Cd Best airfoil	27.09	4.66	0.56%	−17.96%
DO airfoil	30.06	6.51	11.58%	14.61%
Compromised ARO airfoil	28.67	5.32	6.42%	−6.34%

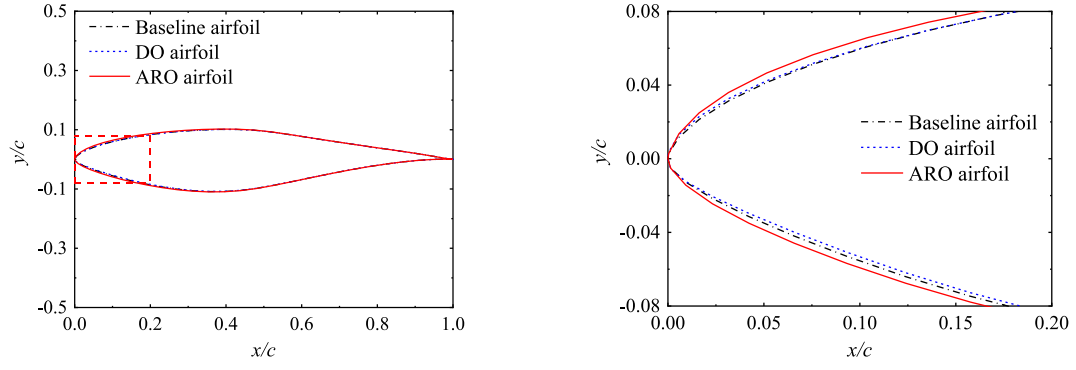

(a) (b)

Fig. 10. Comparisons of airfoil profiles: (a)whole profile; (b) enlarged profile.

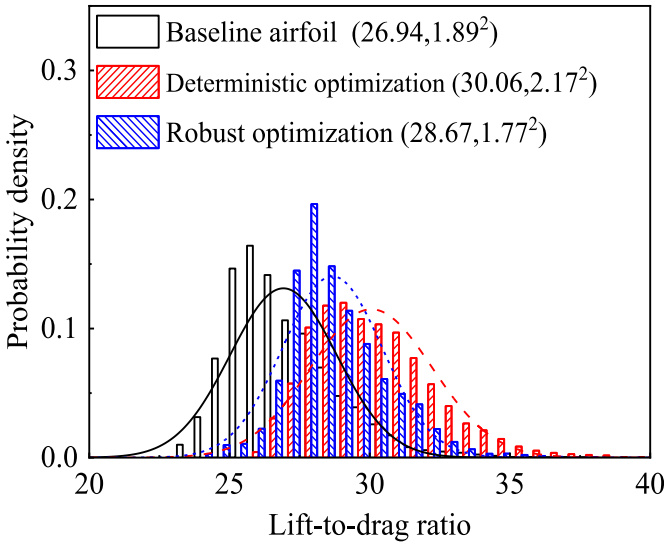

Fig. 11. Comparison of lift drag ratio distributions from Monte Carlo calculations.

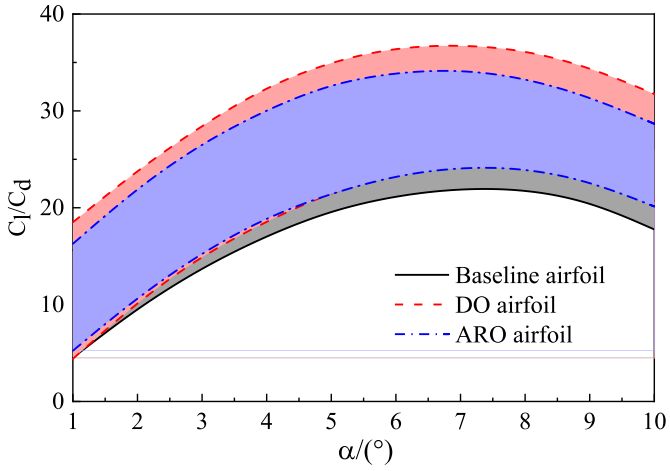

Fig. 12. Lift to drag ratio of three compared airfoils at angle of attack 0–10°.

airfoil with a higher averaged value and lower deviation range of lift to drag ratio is obtained. The results confirm the effectiveness of the proposed ARO approach based on the interval method and Kriging surrogate model.

Table 8 and Fig. 12 compare the lift to drag ratio of the ARO airfoil, the deterministic optimal airfoil and the baseline airfoil at angles of attack of 0–10°. The above three airfoils behaves differently regarding to the maximum lift to drag ratio and its uncertainty. After ARO optimization, the robustness of the airfoil is improved obviously compared to the deterministic optimal airfoil and the baseline airfoil.

4.4. Flow field validation for optimization

In order to further justify the proposed approach, the detailed flow field simulations were conducted at stochastic turbulent condition as described previously. The aerodynamic robustness of the ARO airfoil and the DO airfoil compared to the baseline airfoil were calculated using non-deterministic CFD approach based on the non-intrusive probability collocation method. The mean turbulence is 0.15 and the standard deviation of turbulence is 0.0375. The Reynolds number is 3×10^5 and the angle of attack is 6°.

Fig. 13 plots the standard deviation distribution of pressure coefficient and friction coefficient at the suction side. Compared to the DO airfoil and the baseline airfoil, lower standard deviations of pressure coefficient Cp and friction coefficient Cf are observed for the ARO airfoil, which shows that the aerodynamic robustness of is improved by the proposed ARO approach.

Fig. 14 displays the contour map for the standard deviation distribution of pressure and velocity. It is demonstrated that the uncertainty of flow field of the ARO airfoil is apparently reduced compared to the DO airfoil and the baseline airfoil, which further evidences the improvement of aerodynamic robustness after optimization.

5. Conclusions

This paper innovatively combined the interval analysis with the Kriging model for multiple uncertainty quantification, and presented an aerodynamic robustness optimization approach for wind turbine airfoil considering geometric and inflow uncertainties. The deterministic aerodynamic performance analysis and optimization method is extended and improved to an uncertain analysis and optimization method based on an interval concept. The geometric error uncertainties and the uncertainty of turbulence intensity were described as interval variables. The uncertain aerodynamic response model of airfoil was established based on the interval analysis and a Kriging surrogate model. The uncertainty of aerodynamic performance was obtained by searching the upper limit and the lower limit of the intervals based on generic algorithm. The Kriging surrogate model and the interval analysis were then integrated into the aerodynamic robustness optimization. The ARO optimization objectives were set to maximize the average and to minimize the fluctuation of airfoil performance. The interval analysis method with no need of Gaussian statistical parametrization hypothesis avoids to determine the joint distribution of the correlated multiple uncertain variables. The utilization of interval and Kriging model substitutes massive low-Reynolds-number unsteady flow simulation running in uncertain quantification, therein makes it possible to be integrated into uncertain optimization effectively.

The proposed ARO methodology was thoroughly demonstrated through the benchmarking of wind turbine airfoil S809. Based on the interval analysis and the Kriging model, the uncertain influences on aerodynamic performance of airfoil S809 with different level of uncertainties were investigated. The coupling effects of uncertainties were quantified. The ARO optimization was

Table 8
Lift to drag ratio of three compared airfoils at angle of attack 0–10°from Monte Carlo analysis.

Aifoil	C_l/C_d	1°	2°	3°	4°	5°	6°	7°	8°	9°	10°
Baseline airfoil	Median	10.06	15.52	19.87	23.31	25.62	26.94	27.3	26.79	24.98	21.91
	Uncertainties	±5.55	±5.86	±6.04	±6.18	±5.89	±5.68	±5.29	±4.86	±4.31	±4.15
DO airfoil	Median	11.45	17.09	21.80	25.58	28.37	30.06	30.72	30.36	28.82	26.22
	Uncertainties	±7.05	±6.8	±6.72	±6.95	±6.74	±6.51	±6.14	±5.93	±5.69	±5.53
ARO airfoil	Median	10.76	16.42	21.03	24.60	27.16	28.67	29.26	28.75	27.10	24.40
	Uncertainties	±5.52	±5.66	±5.64	±5.55	±5.66	±5.32	±5.04	±4.65	±4.36	±4.24

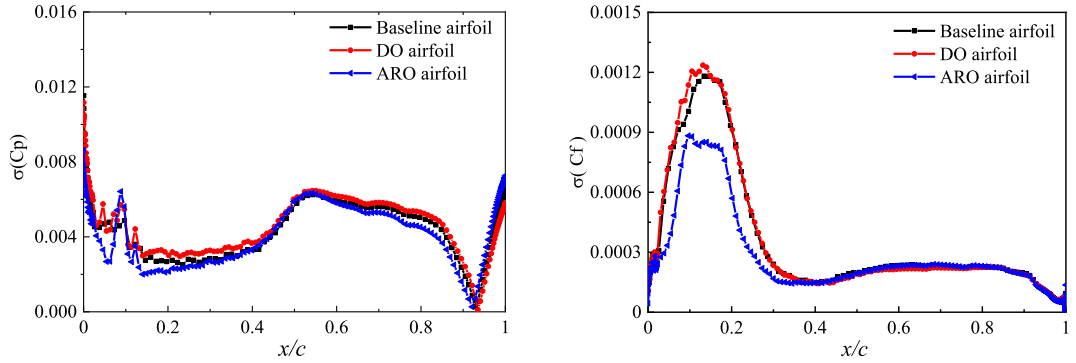

(a) Standard deviation of Cp (b) Standard deviation of Cf

Fig. 13. Comparison of uncertainty distribution of pressure coefficient Cp and friction coefficient Cf at suction side.

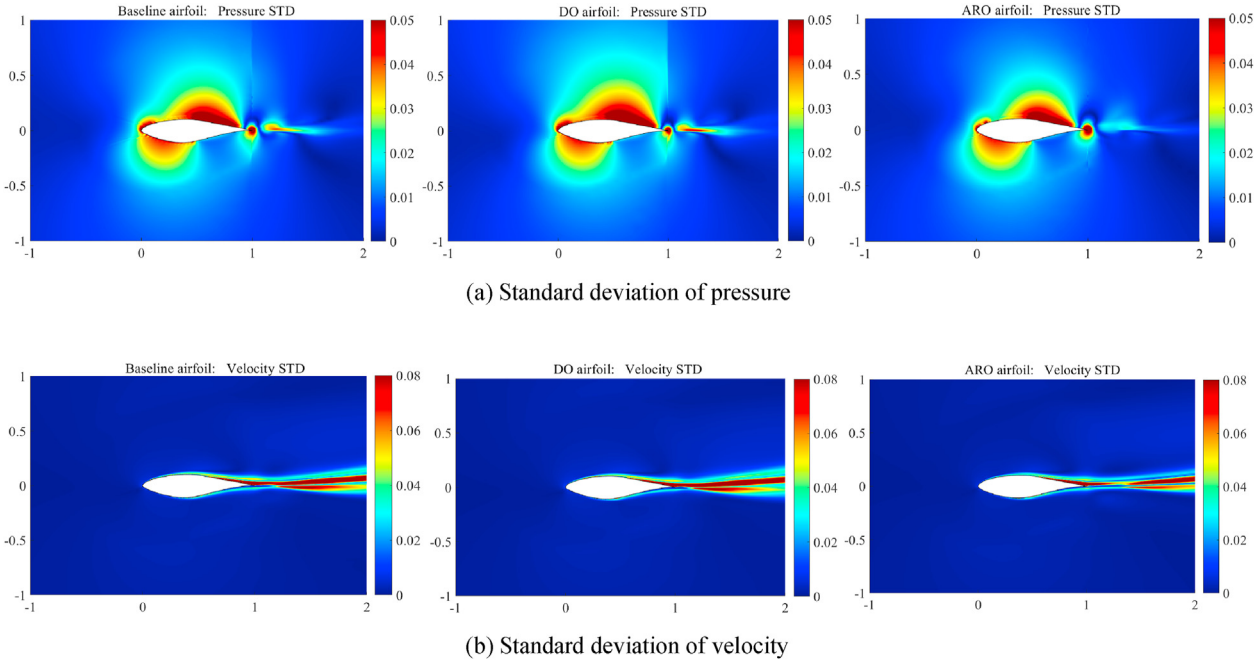

(a) Standard deviation of pressure

(b) Standard deviation of velocity

Fig. 14. Comparison of uncertainty distribution of pressure and velocity.

conducted to maximize the average value of lift to drag ratio and to minimize the fluctuation range of lift to drag ratio, represented by the median value and the radius of the interval of lift to drag ratio. The optimal airfoil was also compared with the deterministic optimal airfoil and the baseline airfoil based on Monte Carlo modelling. The optimization was validated through flow field analysis by non-deterministic CFD approach.

Results show that, the uncertainties of turbulence and geometric error have significant impact on wind turbine airfoil. The pareto frontiers reveal the compromise between maximizing the average value of lift to drag ratio and minimizing the fluctuation interval range of lift to drag ratio. After optimization the min std best airfoil shows 17.96% reduction of fluctuation range and no decreased average of lift to drag ratio compared to the baseline airfoil. While for the compromise design, the interval median of lift to drag ratio increases by 6.42% and the interval radius decreases by 6.34%. The reduced standard deviation distribution of pressure and velocity of the verification case indicates that the sensitivity to the uncertain turbulence is decreased. It is also worth mentioning that the optimization results can be further improved by adding some enhancements to the current approach, such as expanding the design space for the optimization, or using other airfoil parameterization methods.

The method of this paper can further assist in wind turbine design and reliability analysis by expanding the methodology to other components of wind turbine and incorporating various uncertainties. Future work of uncertain quantification and optimization of wind turbine design is currently under taken. This study considers uncertainties associated with wind turbine airfoil, however, the methodology can also be adapted to optimization modelling of other turbomachinery.

Credit author statement

Xinzi Tang: Conceptualization, Methodology, Writing – original draft preparation, Investigation, Writing- Reviewing and Editing. Keren Yuan: Software, Data curation, Investigation. Nengwei Gu: Software, Data curation, Visualization. Pengcheng Li: Visualization, Validation. Ruitao Peng: Reviewing and Editing, Supervision

Declaration of competing interest

The authors declare that they have no known competing financial interests or personal relationships that could have appeared to influence the work reported in this paper.

Acknowledgements

This research was supported by the National Natural Science Foundation of China (Grant No.51975504), the Scientific Research Foundation of Hunan Provincial Education Department (Grant No.19B539), and the Hunan Provincial Natural Science Foundation (Grant No.2021JJ30676).

Nomenclature

ARO	Aerodynamic Robustness Optimization
H−H	Hicks-Henne bump functions
RANS	Reynolds-averaged Naiver-Stokes
CFD	Computational Fluid Dynamics
LHS	Latin Hypercube Samz(x) pling
NSGA-II	Non-dominated Sorting Genetic Algorithm with elitist strategy
MC	Monte Carlo
$y_{up}(x)$	Y-axis coordinates of upper airfoil
$y_{low}(x)$	Y-axis coordinates of lower airfoil
$y_0(x)$	Y-axis coordinates of original airfoil
c_k	coefficient of Hicks-Henne function
x_k	horizontal Control node
n	number of test sample points
c	chord
C_l	Lift coefficient
C_d	Drag coefficient
α	Angle of attack[°]
x	independent variable
$y(x)$	unknown Kriging model
β	regression model parameter
$F(\beta,x)$	regression model which forms the global design space fitting
$z(x)$	a local deviation with a mean of zero and a variance of nonzero
σ	standard deviation
R	correlation matrix
m	number of design variables; median value of interval
θ_k	model parameter
R^2	error squared
y_i	experimental value
$\widehat{y}_i$	estimated value of the surrogate model
$\overline{y}$	mean of the experimental point set
TI	turbulence intensity
C_l/C_d	Lift-to-drag ratio
A^I	interval
A^L	the lower bound of the interval
A^R	the upper bound of the interval
A^C	the median value of the interval
A^W	the radius of the interval
X_{up}	upper airfoil transition position
X_T	maximum relative thickness position
r	radius of interval
$c_{k\ min}$	the lower limits of c_k
$c_{k\ max}$	the upper limits of c_k

References

[1] Pagnini LC, Burlando M, Repetto MP. Experimental power curve of small-size wind turbines in turbulent urban environment. Appl Energy 2015;154:112−21.
[2] Danao LA, Edwards J, Eboibi O, Howell R. A numerical investigation into the influence of unsteady wind on the performance and aerodynamics of a vertical axis wind turbine. Appl Energy 2014;116:111−24.
[3] AbdallahA I, Natarajan J, Sørensen D. Impact of uncertainty in airfoil characteristics on wind turbine extreme loads. Renew Energy 2015;75:283−300.
[4] He X, Li J, Mader CA, Yildirim A, Martins JRRA. Robust aerodynamic shape optimization-From a circle to an airfoil. Aero Sci Technol 2019;87:48−61.
[5] Fusi F, Congedo PM, Guardone A, Quaranta G. Assessment of robust optimization for design of rotorcraft airfoils in forward flight. Aero Sci Technol 2020;107:106355.
[6] Kim D-Y, Kim Y-H, Kim B-S. Changes in wind turbine power characteristics and annual energy production due to atmospheric stability, turbulence intensity, and wind shear. Energy 2021;214:119051.
[7] Gao LY, Liu Y, Zhou WW, Hu H. An experimental study on the aerodynamic performance degradation of a wind turbine blade model induced by ice accretion process. Renew Energy 2019;133:663−75.
[8] Kc A, Whale J, Peinke J. An investigation of the impact of turbulence intermittency on the rotor loads of a small wind turbine. Renew Energy 2021;169:582−97.
[9] Huan Z, Zhenghong G, Yuan G, Chao W. Effective robust design of high lift NLF airfoil under multi-parameter uncertainty. Aero Sci Technol 2017;68:530−42.
[10] He X, Li JAC, Mader A, Yildirim JRR, Martins A. Robust aerodynamic shape optimization-From a circle to an airfoil. Aero Sci Technol 2019;87:48−61.
[11] Hicks RM, Henne PA. Wing design by numerical optimization. J Aircraft 1978;15(7):407−12.
[12] Nemati M, Jahangirian A. Robust aerodynamic morphing shape optimization for high-lift missions. Aero Sci Technol 2020;103:105897.
[13] Tao J, Sun G, Guo LQ, Wang XY. Application of a PCA-DBN-based surrogate model to robust aerodynamic design optimization. Chin J Aeronaut 2020;33(6):1573−88.
[14] Ma C, Gao L, Wang H, Li R, Wu B. Influence of leading edge with real manufacturing error on aerodynamic performance of high subsonic compressor cascades. Chin J Aeronaut 2020. https://doi.org/10.1016/j.cja.2020.08.018.
[15] Zhu JJ, Qiu ZP. Interval analysis for uncertain aerodynamic loads with uncertain-but-bounded parameters. J Fluid Struct 2018;8. 481-436.
[16] Li BY, Wu PG, Li JY, Jiang C. A semi-analytical interval method for response bounds analysis of structures with spatially uncertain loads. Finite Elem Anal Des 2020;182:103483.
[17] Xiong C, Wang L, Liu GH, Shi QH. An iterative dimension-by-dimension method for structural interval response prediction with multidimensional uncertain variables. Aero Sci Technol 2019;86. 572-581.
[18] Kumar PM, Seo J, Seok W, Rhee SH, Samad A. Multi-fidelity optimization of blade thickness parameters for a horizontal axis tidal stream turbine. Renew Energy 2019;135:277−87.
[19] Zou AH, Chassaing JC, Persky R, Gu YT, Sauret E. Uncertainty quantification in high-density fluid radial-inflow turbines for renewable low-grade temperature cycles. Appl Energy 2019;241:313−30.
[20] Wen H, Sang S, Qiu CH, Du XR, Zhu X, Shi Q. A new optimization method of wind turbine airfoil performance based on Bessel equation and GABP artificial neural network. Energy 2019;187:116106.
[21] Salman CA, Thorin E, Yan J. Uncertainty and influence of input parameters and assumptions on the design and analysis of thermochemical waste conversion processes: a stochastic approach. Energy Convers Manag 2020;214:112867.
[22] Langtry RB, Menter FR. Correlation-based transition modeling for unstructured parallelized computational fluid dynamics codes. AIAA J 2009;47(12):2894−906.
[23] Butterfield CP, Musial WP, Simms DA. Combined experiment phase I final report. 1992. p. 257−4655. NREL/TP-257-4655, Golden, Colorado.
[24] Huang CW, Yang K, Liao CC, Wang GF, Zhao XL. Experimental study on aerodynamic characteristics of S809 dedicated wind turbine airfoil at low Reynolds number. Technometrics 2014;35(11):2197−201.
[25] McKay MD, Conover WJ, Beckman RJ. A comparison of three methods for selecting values of input variables in the analysis of output from a computer code. Technometrics 1979;21(2):239−45.
[26] Raul V, Leifsson L. Surrogate-based aerodynamic shape optimization for delaying airfoil dynamic stall using Kriging regression and infill criteria. Aero Sci Technol 2021;111:106555.
[27] Simpson TW, Poplinski J, Koch PN, Allen JK. Metamodels for computer-based engineering design: survey and recommendations. Eng Comput 2001;17(2):129−50.
[28] Osborne WN. Interval analysis introduction,methods and applications. 2017. Nova Science Publishers, Inc.